

Role of Quantum Geometry in the Competition between Higgs Mode and Quasiparticles in Third-Harmonic Generation of Superconductors

Chang-geun Oh,^{1,*} Haruki Watanabe,¹ and Naoto Tsuji^{2,3,4}

¹*Department of Applied Physics, The University of Tokyo, Tokyo 113-8656, Japan*

²*Department of Physics, University of Tokyo, Bunkyo-ku, Tokyo 113-8656, Japan*

³*RIKEN Center for Emergent Matter Science (CEMS), Wako, Saitama 351-0198, Japan*

⁴*Trans-scale Quantum Science Institute, University of Tokyo, Bunkyo-ku, Tokyo 113-8656, Japan*

Collective modes in superconductors, such as the Higgs mode, offer deep insights into the nature of condensates. Third-harmonic generation (THG) is a primary tool for probing the Higgs mode, but its signal competes with that of quasiparticle excitations depending on impurity scattering rates. In particular, in the clean regime the standard BCS theory generally predicts the dominance of quasiparticle contributions. Here, we propose and demonstrate that the quantum geometry of electronic bands can be a key mechanism governing this competition. By developing a formalism that explicitly incorporates the quantum metric, and applying it to a tunable model of a dispersive-band superconductor, we show that the quantum metric can dramatically amplify the nonlinear light-Higgs coupling by several orders of magnitude. Our results establish that a large quantum metric can cause the Higgs mode to dominate the THG response, resolving the puzzle of Higgs and quasiparticle competition in the clean regime and identifying band geometry as a crucial ingredient for designing and understanding the nonlinear response of superconductors.

Introduction. Superconductors are not merely perfect conductors but represent a macroscopic quantum state formed by the condensation of Cooper pairs [1, 2]. As a consequence of this phase transition, superconductors host unique collective excitation modes, such as the amplitude fluctuation known as the Higgs mode and the phase fluctuation known as the Nambu-Goldstone mode [3–7]. In charged systems, the phase mode is pushed to a high-energy scale, corresponding to the plasma frequency, by the Anderson-Higgs mechanism [8–11]. In contrast, the Higgs mode remains a gapped excitation near the superconducting gap energy, 2Δ . Since the Higgs mode does not linearly couple to external electromagnetic fields under general circumstances, its observation has primarily relied on nonlinear response techniques, such as Raman scattering [12–14], third-harmonic generation (THG) [15–20], and pump-probe spectroscopy [15, 21–23].

The THG signal, which appears under the resonance condition $2\Omega = 2\Delta$ (where Ω is the frequency of the incident light), has been considered a powerful tool for probing the existence of the Higgs mode [15, 24]. However, this energy regime is also the threshold for the pair-breaking process of quasiparticles, making it a significant challenge to distinguish between the two contributions. According to the standard BCS theory for single-band superconductors in the clean limit, the THG signal is expected to be predominantly governed by quasiparticle excitations [25].

However, experiments on materials such as NbN have indicated that the Higgs mode in fact dominates the THG resonance; this is supported by polarization-angle dependence measurements of THG [16] and a comparison to first-principles-based calculations including impurity scattering [26]. In fact, the contribution of the Higgs mode to THG is strongly enhanced with the help of impurities [26–31] or phonon retardation effects [32], since the paramagnetic

coupling to electromagnetic fields is allowed in those situations. While this mechanism is plausible, the interpretation of experimental results often requires a detailed comparison to material-specific theoretical calculations. Thus, a universal, material-independent principle governing the competition between the Higgs and quasiparticle channels has remained a key open question in the field [33].

Recently, the quantum geometry of electronic wavefunctions has emerged as a crucial factor in understanding various phenomena in condensed matter [34–37]. The geometry of quantum states is described by the quantum geometric tensor, whose symmetric real part is the quantum metric, and whose antisymmetric imaginary part is the Berry curvature [38–40]. While the role of the Berry curvature is well-established as a cornerstone of topological physics [41, 42], the physical consequences of the quantum metric have only recently begun to be explored in depth, with significant implications for superfluidity [34, 35, 43–46], optical responses [47–56], magnetic properties [57–59], and other electronic properties [60–65]. The profound impact of quantum geometry on superconductivity has been particularly highlighted in the context of flat-band systems, where the quantum metric, rather than band dispersion, governs the superfluid weight [34, 35, 43]. A recent study suggested that this could also significantly influence the Higgs mode in such flat-band systems [66]. However, the role of quantum geometry in conventional superconductors with dispersive bands—which constitute the vast majority of known materials—remains a largely unexplored and crucial question in the context of nonlinear optics, especially for its influence on collective modes like the Higgs mode.

In this paper, we show that the quantum geometry of the electronic wavefunction plays a key role in determining the relative contributions of the Higgs mode and quasiparticles in the THG response. We demonstrate that the light-matter interaction mediated by this quantum metric acts asymmetrically on the Higgs mode and quasiparticle channels, leading to a dramatic amplification of the nonlinear optical response of the Higgs mode.

* cg.oh.0404@gmail.com

Formalism.

We begin with a Hamiltonian for a multiband system (setting $\hbar = e = c = 1$),

$$\mathcal{H} = \mathcal{H}_0 + \mathcal{H}_{\text{int}}, \quad (1)$$

$$\mathcal{H}_0 = \sum_{\mathbf{k}\sigma\alpha\beta} c_{\mathbf{k}\alpha\sigma}^\dagger \mathcal{H}_{\alpha\beta}^\sigma(\mathbf{k}) c_{\mathbf{k}\beta\sigma}, \quad (2)$$

$$\mathcal{H}_{\text{int}} = - \sum_{\mathbf{k}\mathbf{k}'\alpha\beta} U_{\alpha\beta} c_{\mathbf{k}\alpha\uparrow}^\dagger c_{-\mathbf{k}\beta\downarrow}^\dagger c_{-\mathbf{k}'\beta\downarrow} c_{\mathbf{k}'\alpha\uparrow}. \quad (3)$$

Introducing the path integral and decoupling the interaction in the pairing channel by a Hubbard–Stratonovich field $\Delta_{\alpha\beta}(\tau)$ yields the action $S[c^\dagger, c, \Delta^*, \Delta]$; we defer standard steps to the Supplemental Material.

Minimal coupling to an external spatially uniform vector potential $\mathbf{A}(\tau)$ is implemented by $\mathbf{k} \rightarrow \mathbf{k} - \mathbf{A}(\tau)$ in \mathcal{H}_0 . Note that for nonlocal electron interactions, the pairing function itself can couple to the gauge field [67]. Assuming a local pairing interaction, only the kinetic term is modified by the vector potential. Diagonalizing \mathcal{H}_0 at each \mathbf{k} provides band eigenstates $|u_{l\sigma}(\mathbf{k})\rangle$ and dispersions $\epsilon_{l\sigma}(\mathbf{k})$. We assume (i) time-reversal and inversion symmetry for the normal-state band, (ii) a single band (labeled m , which we drop hereafter) dominates at the Fermi level, and (iii) uniform intra-orbital pairing $\Delta_{\alpha\beta} = \Delta\delta_{\alpha\beta}$, a key condition that renders the quantum geometric contribution manifest [34, 35, 46]. Under these assumptions we project onto the single active band and obtain the effective low-energy action

$$S = \int_0^\beta d\tau \left\{ N_b \frac{|\Delta|^2}{U} + \sum_{\mathbf{k},\sigma} c_\sigma^\dagger(\mathbf{k}) [\partial_\tau + \epsilon_\sigma(\mathbf{k} - \mathbf{A}) - \mu] c_\sigma(\mathbf{k}) - \sum_{\mathbf{k}} [\Delta f(\mathbf{k}, \mathbf{A}) c_\uparrow^\dagger(\mathbf{k}) c_\downarrow^\dagger(-\mathbf{k}) + \text{h.c.}] \right\}, \quad (4)$$

where N_b is the number of orbitals and the pairing overlap is

$$f(\mathbf{k}, \mathbf{A}) = \sum_{\alpha} u_{\alpha}^*(\mathbf{k} + \mathbf{A}) u_{\alpha}(\mathbf{k} - \mathbf{A}) = \langle u_{\mathbf{k}+\mathbf{A}} | u_{\mathbf{k}-\mathbf{A}} \rangle. \quad (5)$$

For a long-wavelength vector potential, we Taylor-expand $f(\mathbf{k}, \mathbf{A})$. With time-reversal and inversion symmetry, the expansion reveals the quantum metric:

$$|f(\mathbf{k}, \mathbf{A})| \approx 1 - 2 g_{ij}(\mathbf{k}) A_i A_j + \mathcal{O}(A^4), \quad (6)$$

with the quantum metric defined as $g_{ij}(\mathbf{k}) = \text{Re} \langle \partial_i u_{\mathbf{k}} | (1 - P_{\mathbf{k}}) | \partial_j u_{\mathbf{k}} \rangle$, where $P_{\mathbf{k}} = |u_{\mathbf{k}}\rangle \langle u_{\mathbf{k}}|$ is the projection operator onto the Bloch state.

Introducing the Nambu spinor $\psi_{\mathbf{k}}(\tau) = (c_{\uparrow}(\mathbf{k}), c_{\downarrow}^\dagger(-\mathbf{k}))^T$, the inverse Nambu Green's function reads

$$\mathcal{G}^{-1}(\mathbf{k}, \tau) = -\partial_\tau \tau_0 - \xi_{\mathbf{k}} \tau_3 + \Delta_0 \tau_1 - \Sigma(\mathbf{k}, \tau), \quad (7)$$

where $\xi_{\mathbf{k}} = \epsilon_{\mathbf{k}} - \mu$ and the self-energy due to amplitude fluctuation $\rho(\tau)$ and the electromagnetic field (up to $\mathcal{O}(A^2)$) is

$$\begin{aligned} \Sigma(\mathbf{k}, \tau) = & \rho(\tau) \tau_1 + \frac{1}{2} \partial_{ij}^2 \xi_{\mathbf{k}} A_i(\tau) A_j(\tau) \tau_3 \\ & + 2(\Delta_0 + \rho(\tau)) g_{ij}(\mathbf{k}) A_i(\tau) A_j(\tau) \tau_1. \end{aligned} \quad (8)$$

Expanding the fermion determinant to quartic order in fields and integrating out the fermions and the Higgs field ρ gives the effective electromagnetic action

$$S[A] = \sum_{ijkl} \int d\omega A_{ij}^2(-\omega) K_{ijkl}(\omega) A_{kl}^2(\omega). \quad (9)$$

The optical kernel $K_{ijkl}(\omega)$ is the central result of our formalism; it decomposes into contributions from quasiparticles (qp) and the Higgs mode, $K_{ijkl} = K_{ijkl}^{\text{qp}} + K_{ijkl}^{\text{Higgs}}$. Crucially, each of these contributions can be further separated into a conventional term from the band dispersion (band) and a novel term from the quantum geometry (geom).

The quasiparticle contribution is explicitly decomposed as

$$\begin{aligned} K_{ijkl}^{\text{qp}}(\omega) = & \underbrace{\sum_{\mathbf{k}} \frac{1}{4} \partial_{ij}^2 \xi_{\mathbf{k}} \partial_{kl}^2 \xi_{\mathbf{k}} \chi_{33}(\mathbf{k}, \omega)}_{K_{\text{band}}^{\text{qp}}} \\ & + \underbrace{\sum_{\mathbf{k}} 2\Delta_0 \partial_{ij}^2 \xi_{\mathbf{k}} g_{kl}(\mathbf{k}) \chi_{13}(\mathbf{k}, \omega) + 4\Delta_0^2 g_{ij}(\mathbf{k}) g_{kl}(\mathbf{k}) \chi_{11}(\mathbf{k}, \omega)}_{K_{\text{geom}}^{\text{qp}}}, \end{aligned} \quad (10)$$

and the Higgs-mediated contribution reads

$$K_{ijkl}^{\text{Higgs}}(\omega) = -V_{ij}(\omega) \mathcal{G}_H^0(\omega) V_{kl}(\omega), \quad (11)$$

where $\mathcal{G}_H^0(\omega)$ is the bare propagator for the Higgs amplitude mode. The Higgs-light coupling vertex $V_{ij}(\omega)$ itself contains both band and geometric parts:

$$V_{ij}(\omega) = \underbrace{\frac{1}{2} \sum_{\mathbf{k}} \partial_{ij}^2 \xi_{\mathbf{k}} \chi_{13}(\mathbf{k}, \omega)}_{V_{ij}^{\text{band}}} + \underbrace{2\Delta_0 \sum_{\mathbf{k}} g_{ij}(\mathbf{k}) \chi_{11}(\mathbf{k}, \omega)}_{V_{ij}^{\text{geom}}}. \quad (12)$$

The bubble functions $\chi_{\alpha\beta}$ are defined in Matsubara frequency as $\chi_{\alpha\beta}(\mathbf{k}, i\omega_m) = \frac{1}{\beta} \sum_{i\omega_n} \text{Tr} [\mathcal{G}_0(\mathbf{k}, i\omega_n) \tau_\alpha \mathcal{G}_0(\mathbf{k}, i\omega_n + i\omega_m) \tau_\beta]$, with \mathcal{G}_0 being the mean-field Nambu Green's function. Finally, the third-harmonic current for a monochromatic drive $A_i(t) = a_i e^{-i\Omega t} + a_i^* e^{i\Omega t}$ is obtained by functional differentiation $j_m(t) = -\delta S / \delta A_m(t)$:

$$j_m(3\Omega) = -4 \sum_{jkl} [K_{mjkl}^{\text{qp}}(2\Omega) + K_{mjkl}^{\text{Higgs}}(2\Omega)] a_j a_k a_l. \quad (13)$$

Application to a Quadratic Band Touching Model.

To isolate the role of quantum geometry, we employ a specially designed two-band model that hosts a quadratic band touching at the Γ point ($\mathbf{k} = 0$). The explicit form and details are described in the SI. The model is constructed to produce a familiar energy band dispersions, given by $E_+(\mathbf{k}) = -2t(\cos k_x + \cos k_y)$ and $E_-(\mathbf{k}) = -2t_b(\cos k_x + \cos k_y) + 4(t_b - t)$, as shown in Fig. 1(a). A key feature of this model is that these energy dispersions remain fixed while the quantum geometry of the Bloch states is continuously tuned by

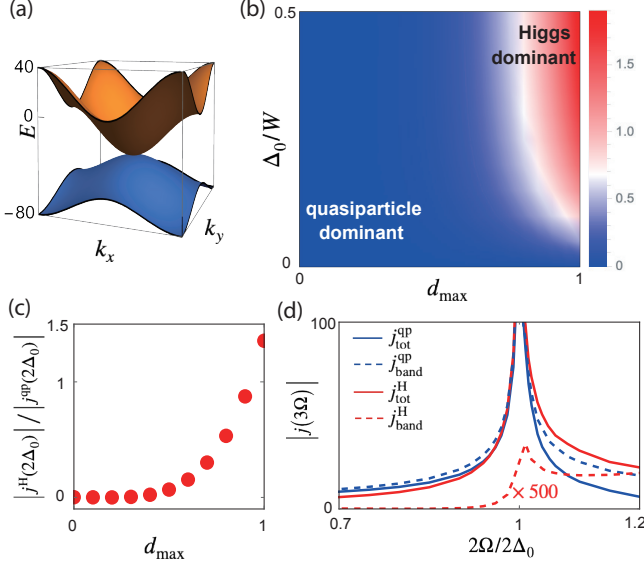


FIG. 1. Quantum geometric enhancement of the Higgs mode in the THG response. (a) Energy band dispersions of the quadratic band touching model with $t = 10$ and $t_b = -5$. (b) Crossover diagram of the THG intensity ratio $|J_{\text{tot}}^H|/|J_{\text{tot}}^{\text{qp}}|$ versus the quantum geometry parameter d_{max} and the gap to band width Δ_0/W , where $W = 8t$ is the band width of the upper band. (c) The ratio of the THG peak heights at resonance as a function of d_{max} for a fixed dispersion, quantifying the crossover from quasiparticle to Higgs dominance. (d) THG spectrum in the Higgs-dominant regime at $d_{\text{max}} = 1$. Solid (dashed) lines represent the total (band-only) contributions for the Higgs (red) and quasiparticle (blue) channels. The band-only Higgs contribution is magnified by $\times 500$ for visibility, highlighting that the geometric terms are responsible for the enhancement. Here, the results in (b-d) were calculated with $\mu = -3t$ and in (c,d) we set $\Delta_0/W = 0.1$.

a parameter $d_{\text{max}} \in [0, 1]$, which physically corresponds to the maximum quantum distance between Bloch states within the same band over the Brillouin zone and directly controls the quantum metric [47, 60, 63]. Since all components of the quantum metric are proportional to its square ($g_{ij} \propto d_{\text{max}}^2$), $d_{\text{max}} = 0$ defines a geometrically trivial model, while $d_{\text{max}} = 1$ represents a maximally nontrivial case. This construction allows us to systematically isolate geometric effects on the THG response.

In our analysis, we focus exclusively on the upper electronic band, $E_+(\mathbf{k})$, (assuming $t_b < 0$) and consider the Fermi level sufficiently far from the band touching point at $\mathbf{k} = \mathbf{0}$. Provided that the superconducting gap and relevant excitation energies satisfy $\Delta_0, \hbar\Omega, k_B T \ll \min_{\mathbf{k} \in \text{FS}} |E_+(\mathbf{k}) - E_-(\mathbf{k})|$, interband pairing and virtual interband transitions are negligible, and the single-band effective theory introduced in the previous section is justified.

Our central finding using this model is that the quantum geometry, tuned by the parameter d_{max} , decisively controls the relative strength of the Higgs mode and quasiparticle contributions to the nonlinear response. This geometry-driven effect is then significantly amplified by the ratio of the superconducting gap to the bandwidth Δ_0/W , where $W = 8t$ is the band

width. The key results are summarized in Fig. 1. Figure 1(b) presents a crossover diagram for the ratio of the THG intensity from the Higgs mode to that from quasiparticles, $|J_{\text{tot}}^H|/|J_{\text{tot}}^{\text{qp}}|$, as a function of the quantum geometry parameter d_{max} and the gap Δ_0/W . For this calculation, we set the chemical potential to $\mu = -3t$. The primary trend, observed by moving horizontally, is a transition from a quasiparticle-dominant regime (blue) at small d_{max} to a Higgs-dominant regime (red) as the geometric contribution increases. Crucially, the influence of quantum geometry is enhanced in systems with flatter bands. As Δ_0/W increases (moving vertically), the crossover to Higgs dominance occurs at a smaller critical value of d_{max} . This demonstrates that a flatter band structure makes the non-linear response more sensitive to quantum geometry, providing a clear connection to the flat-band limit ($\Delta_0/W \gg 1$). Indeed, it has been recently shown for ideal flat-band systems that the THG response is almost entirely attributed to the Higgs mode, with the quasiparticle contribution being negligible due to quantum geometric effects [66].

The dramatic enhancement by geometry is quantified in Fig. 1(c), which shows the ratio of the peak heights at resonance as a function of d_{max} for a fixed $\Delta_0/W = 0.1$. For negligible geometric effects ($d_{\text{max}} \rightarrow 0$), the Higgs contribution is heavily suppressed, with the ratio being on the order of $\approx 10^{-3}$, consistent with expectations from conventional theories where quasiparticle channels dominate. However, as d_{max} increases, the ratio grows by several orders of magnitude, demonstrating a dramatic enhancement of the Higgs-mediated THG response driven by the quantum geometry.

The impact on the THG spectrum is shown in Fig. 1(d) for $\Delta_0/W = 0.1$ and $d_{\text{max}} = 1$ within the Higgs-dominant regime. The red and blue solid lines represent the total contributions from the Higgs (j_{tot}^H) and quasiparticle ($j_{\text{tot}}^{\text{qp}}$) channels, while the dashed lines show the conventional (trivial) band-only contributions (j_{band}). At the resonance ($2\Omega/2\Delta_0 \approx 1$), the total Higgs response is significantly larger than the total quasiparticle response. Notably, comparing the solid and dashed lines reveals that this enhancement originates almost entirely from the quantum geometric terms. The conventional band-only contribution for the Higgs mode (j_{band}^H) is extremely small and has been magnified by a factor of 500 for visibility. Therefore, our results clearly identify the quantum geometry of the Bloch states as the primary mechanism responsible for amplifying the Higgs mode's signature in the nonlinear optical response.

Correlation length. Beyond the electromagnetic response, the quantum geometry of the Bloch states also fundamentally determines the spatial properties of the Higgs mode, such as its correlation length ξ_H [66], the characteristic spatial scale over which fluctuations in the amplitude of the superconducting order parameter remain correlated. To investigate this, we analyze the effective action for the order parameter fluctuations in the absence of an external field ($\mathbf{A} = 0$), focusing on the static, long-wavelength limit. As detailed in the Supplemental Material, by expanding the effective action for the amplitude mode $\rho(\mathbf{q})$ to second order in momentum \mathbf{q} , we obtain a Ginzburg-Landau-type propagator $\langle \rho(\mathbf{q})\rho(-\mathbf{q}) \rangle \propto (r_\rho + A_{ij}q_i q_j)^{-1}$. From this, the Higgs correlation length

tensor is identified as $\xi_{H,ij}^2 = A_{ij}/r_\rho$.

Similar to the optical kernel, the stiffness tensor A_{ij} can be decomposed into a part from the band dispersion and a part from the quantum geometry:

$$\xi_{H,ij}^2 = \xi_{\text{band},ij}^2 + \xi_{\text{geom},ij}^2, \quad (14)$$

where the explicit form of each term is given in the Supplemental Material. The geometric contribution $\xi_{\text{geom},ij}^2$ is directly related to the quantum metric $g_{ij}(\mathbf{k})$.

We now quantify the geometric contribution to the correlation length using the quadratic band touching model. The calculation uses the same parameters as in the THG analysis in Fig. 1(c,d). Since the band dispersion in our model is independent of d_{max} , the band contribution $\xi_{\text{band},xx}^2$ remains constant. Therefore, any variation in the total correlation length directly measures the effect of quantum geometry. Figure 2(a) shows the calculated total squared correlation length, $\xi_{H,xx}^2$, which increases monotonically as a function of d_{max} . To illustrate the dramatic crossover in the underlying contributions, we plot the ratio $\xi_{\text{geom},xx}^2/\xi_{\text{band},xx}^2$ in Fig. 2(b). The ratio grows from zero to a value greater than one, signifying a clear transition from a band-dominated regime to one where the correlation length is overwhelmingly determined by quantum geometry. This result unequivocally demonstrates that the quantum metric provides a significant contribution to the stiffness of the Higgs mode. While the stiffness against spatial variations of the order parameter's amplitude is primarily determined by the kinetic energy of electrons, our finding reveals that the geometric properties of the Bloch wavefunctions themselves provide an additional contribution to this stiffness. This enhancement of the correlation length is a direct manifestation of how the underlying geometry of the quantum states governs the macroscopic rigidity of the superconducting condensate's amplitude.

To complement the above discussion of the Higgs correlation length and the stiffness tensor A_{ij} , we evaluate the superfluid stiffness D_{ij} for our model. The superfluid stiffness D_{ij} decomposes into a conventional band contribution and a quantum-geometry contribution, $D_{ij} = D_{ij}^{\text{band}} + D_{ij}^{\text{geom}}$ [34, 43]. The geometric part increases as d_{max} increases, indicating that parameter regimes with an enhanced quantum metric not only strengthen the geometric part of A_{ij} but also increase the superfluid stiffness. Detailed expressions and the d_{max} -dependence are provided in SI.

Conclusion. In this work, we have theoretically investigated the role of quantum geometry in the nonlinear optical response of superconductors, focusing on the competition between the Higgs mode and quasiparticle contributions to THG. By developing a formalism based on a single-band projection of a multiband Hamiltonian, we explicitly derived the THG optical kernel, systematically decomposing it into band and geometric contributions. Applying our formalism to a tunable quadratic band touching model, where the quan-

tum geometry can be varied independently of the band structure, we have demonstrated that the quantum metric provides a significant contribution to the nonlinear light-matter coupling. Our key finding is that a prominent quantum geometry can enhance the THG response of the Higgs mode by several orders

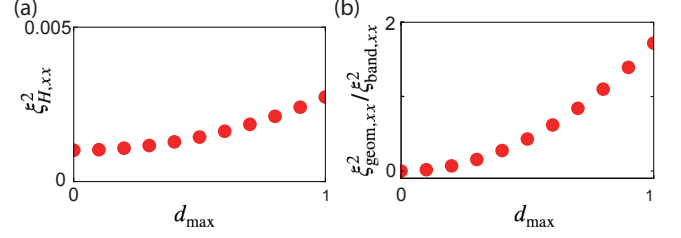


FIG. 2. Quantum geometric enhancement of the correlation length for the Higgs mode. (a) The total squared correlation length of the Higgs mode, $\xi_{H,xx}^2$, as a function of the quantum geometry parameter d_{max} within the quadratic band touching model. (b) The ratio of the geometric to the band contribution to the squared correlation length, $\xi_{\text{geom},xx}^2/\xi_{\text{band},xx}^2$. The parameters $\mu, \Delta_0/W$ are the same as in Fig. 1(b,c).

of magnitude. Furthermore, we have shown that the Higgs correlation length is also enhanced by the quantum geometry, directly linking the spatial rigidity of the condensate's amplitude to the underlying wavefunction geometry.

Our findings provide a fundamental and general mechanism that can enhance the Higgs-mode contribution to THG. While previous theories have invoked impurity scattering or phonon retardation effects that may depend on material details, our work suggests that a large quantum metric can be a universal principle for achieving a strong Higgs response in dispersive-band systems in the clean regime. This shifts the focus from extrinsic factors to an intrinsic, geometric property of the electronic states themselves.

Experimentally, our work calls for a targeted search for strong Higgs responses in materials known to possess a large quantum metric, such as those with nearly flat bands. Probing the THG response while tuning the quantum geometry—for instance, by applying an electric field or strain—could provide a direct verification of our theory. Ultimately, our study establishes the engineering of quantum geometry as a new and promising route for controlling and amplifying the collective dynamics of superconductors.

ACKNOWLEDGMENTS

The authors thank J. Rhim for useful discussions. C.O. was supported by JSPS KAKENHI Grant No. JP25KF0186. H. W. was supported by JSPS KAKENHI grant No. JP24K00541. N.T. acknowledges support by JST FOREST (Grant No. JPMJFR2131) and JSPS KAKENHI (Grant Nos. JP24H00191, JP25H01246, JP25H01251).

[1] M. Tinkham, *Introduction to superconductivity* (Courier Corporation, 2004).

[2] J. Bardeen, L. N. Cooper, and J. R. Schrieffer, Theory of super-

- conductivity, Phys. Rev. **108**, 1175 (1957).
- [3] P. W. Anderson, Random-phase approximation in the theory of superconductivity, Phys. Rev. **112**, 1900 (1958).
 - [4] A. Schmid, The Approach to Equilibrium in a Pure Superconductor: The Relaxation of the Cooper Pair Density, Phys. Kondens. Mater. **8**, 129 (1968).
 - [5] D. Pekker and C. Varma, Amplitude/Higgs modes in condensed matter physics, Annu. Rev. Condens. Matter Phys. **6**, 269 (2015).
 - [6] R. Shimano and N. Tsuji, Higgs mode in superconductors, Annu. Rev. Condens. Matter Phys. **11**, 103 (2020).
 - [7] N. Tsuji, I. Danshita, and S. Tsuchiya, Higgs and Nambu–Goldstone modes in condensed matter physics, in *Encyclopedia of Condensed Matter Physics (Second Edition)* (Academic Press, Oxford, 2024) 2nd ed., pp. 174–186.
 - [8] P. W. Anderson, Plasmons, gauge invariance, and mass, Phys. Rev. **130**, 439 (1963).
 - [9] F. Englert and R. Brout, Broken Symmetry and the Mass of Gauge Vector Mesons, Phys. Rev. Lett. **13**, 321 (1964).
 - [10] P. W. Higgs, Broken Symmetries and the Masses of Gauge Bosons, Phys. Rev. Lett. **13**, 508 (1964).
 - [11] G. S. Guralnik, C. R. Hagen, and T. W. B. Kibble, Global Conservation Laws and Massless Particles, Phys. Rev. Lett. **13**, 585 (1964).
 - [12] R. Sooryakumar and M. V. Klein, Raman Scattering by Superconducting-Gap Excitations and Their Coupling to Charge-Density Waves, Phys. Rev. Lett. **45**, 660 (1980).
 - [13] M.-A. Méasson, Y. Gallais, M. Cazayous, B. Clair, P. Rodière, L. Cario, and A. Sacuto, Amplitude Higgs mode in the $2H$ – $NbSe_2$ superconductor, Phys. Rev. B **89**, 060503 (2014).
 - [14] R. Grasset, Y. Gallais, A. Sacuto, M. Cazayous, S. Mañas Valero, E. Coronado, and M.-A. Méasson, Pressure-Induced Collapse of the Charge Density Wave and Higgs Mode Visibility in $2H$ – TaS_2 , Phys. Rev. Lett. **122**, 127001 (2019).
 - [15] R. Matsunaga, N. Tsuji, H. Fujita, A. Sugioka, K. Makise, Y. Uzawa, H. Terai, Z. Wang, H. Aoki, and R. Shimano, Light-induced collective pseudospin precession resonating with Higgs mode in a superconductor, Science **345**, 1145 (2014).
 - [16] R. Matsunaga, N. Tsuji, K. Makise, H. Terai, H. Aoki, and R. Shimano, Polarization-resolved terahertz third-harmonic generation in a single-crystal superconductor NbN: Dominance of the Higgs mode beyond the BCS approximation, Phys. Rev. B **96**, 020505 (2017).
 - [17] H. Chu, M.-J. Kim, K. Katsumi, S. Kovalev, R. D. Dawson, L. Schwarz, N. Yoshikawa, G. Kim, D. Putzky, Z. Z. Li, H. Raffy, S. Germanskiy, J.-C. Deinert, N. Awari, I. Ilyakov, B. Green, M. Chen, M. Bawatna, G. Cristiani, G. Logvenov, Y. Gallais, A. V. Boris, B. Keimer, A. P. Schnyder, D. Manske, M. Gensch, Z. Wang, R. Shimano, and S. Kaiser, Phase-resolved Higgs response in superconducting cuprates, Nat. Commun. **11**, 1793 (2020).
 - [18] S. Kovalev, T. Dong, L.-Y. Shi, C. Reinhofer, T.-Q. Xu, H.-Z. Wang, Y. Wang, Z.-Z. Gan, S. Germanskiy, J.-C. Deinert, I. Ilyakov, P. H. M. van Loosdrecht, D. Wu, N.-L. Wang, J. Demsar, and Z. Wang, Band-selective third-harmonic generation in superconducting MgB_2 : Possible evidence for the Higgs amplitude mode in the dirty limit, Phys. Rev. B **104**, L140505 (2021).
 - [19] Z.-X. Wang, J.-R. Xue, H.-K. Shi, X.-Q. Jia, T. Lin, L.-Y. Shi, T. Dong, F. Wang, and N.-L. Wang, Transient Higgs oscillations and high-order nonlinear light-Higgs coupling in a terahertz wave driven NbN superconductor, Phys. Rev. B **105**, L100508 (2022).
 - [20] M.-J. Kim, S. Kovalev, M. Udina, R. Haenel, G. Kim, M. Puviani, G. Cristiani, I. Ilyakov, T. V. A. G. de Oliveira, A. Ponomaryov, J.-C. Deinert, G. Logvenov, B. Keimer, D. Manske, L. Benfatto, and S. Kaiser, Tracing the dynamics of superconducting order via transient terahertz third-harmonic generation, Sci. Adv. **10**, eadi7598 (2024).
 - [21] R. Matsunaga, Y. I. Hamada, K. Makise, Y. Uzawa, H. Terai, Z. Wang, and R. Shimano, Higgs Amplitude Mode in the BCS Superconductors $Nb_{1-x}Ti_xN$ Induced by Terahertz Pulse Excitation, Phys. Rev. Lett. **111**, 057002 (2013).
 - [22] K. Katsumi, N. Tsuji, Y. I. Hamada, R. Matsunaga, J. Schneeloch, R. D. Zhong, G. D. Gu, H. Aoki, Y. Gallais, and R. Shimano, Higgs Mode in the d -Wave Superconductor $Bi_2Sr_2CaCu_2O_{8+x}$ Driven by an Intense Terahertz Pulse, Phys. Rev. Lett. **120**, 117001 (2018).
 - [23] C. Vaswani, J. H. Kang, M. Mootz, L. Luo, X. Yang, C. Sundahl, D. Cheng, C. Huang, R. H. J. Kim, Z. Liu, Y. G. Collantes, E. E. Hellstrom, I. E. Perakis, C. B. Eom, and J. Wang, Light quantum control of persisting Higgs modes in iron-based superconductors, Nat. Commun. **12**, 258 (2021).
 - [24] N. Tsuji and H. Aoki, Theory of Anderson pseudospin resonance with Higgs mode in superconductors, Phys. Rev. B **92**, 064508 (2015).
 - [25] T. Cea, C. Castellani, and L. Benfatto, Nonlinear optical effects and third-harmonic generation in superconductors: Cooper pairs versus Higgs mode contribution, Phys. Rev. B **93**, 180507 (2016).
 - [26] N. Tsuji and Y. Nomura, Higgs-mode resonance in third harmonic generation in NbN superconductors: Multiband electron-phonon coupling, impurity scattering, and polarization-angle dependence, Phys. Rev. Res. **2**, 043029 (2020).
 - [27] T. Jujo, Quasiclassical Theory on Third-Harmonic Generation in Conventional Superconductors with Paramagnetic Impurities, J. Phys. Soc. Jpn. **87**, 024704 (2018).
 - [28] Y. Murotani and R. Shimano, Nonlinear optical response of collective modes in multiband superconductors assisted by non-magnetic impurities, Phys. Rev. B **99**, 224510 (2019).
 - [29] M. Silaev, Nonlinear electromagnetic response and Higgs-mode excitation in BCS superconductors with impurities, Phys. Rev. B **99**, 224511 (2019).
 - [30] G. Seibold, M. Udina, C. Castellani, and L. Benfatto, Third harmonic generation from collective modes in disordered superconductors, Phys. Rev. B **103**, 014512 (2021).
 - [31] P. Derendorf, A. F. Volkov, and I. M. Eremin, Nonlinear response of diffusive superconductors to ac electromagnetic fields, Phys. Rev. B **109**, 024510 (2024).
 - [32] N. Tsuji, Y. Murakami, and H. Aoki, Nonlinear light-Higgs coupling in superconductors beyond BCS: Effects of the retarded phonon-mediated interaction, Phys. Rev. B **94**, 224519 (2016).
 - [33] Another recent approach to address this question is the two-dimensional terahertz coherent spectroscopy [68–70]. However, it has been pointed out that there is also a similar competition between the Higgs mode and quasiparticle excitations in the two-dimensional coherent spectroscopy for disordered superconductors [71].
 - [34] S. Peotta and P. Törmä, Superfluidity in topologically nontrivial flat bands, Nat. Commun. **6**, 8944 (2015).
 - [35] P. Törmä, S. Peotta, and B. A. Bernevig, Superconductivity, superfluidity and quantum geometry in twisted multilayer systems, Nat. Rev. Phys. **4**, 528 (2022).
 - [36] J. Yu, B. A. Bernevig, R. Queiroz, E. Rossi, P. Törmä, and B.-J. Yang, Quantum geometry in quantum materials, arXiv preprint arXiv:2501.00098 (2024).

- [37] P. Törmä, Essay: Where can quantum geometry lead us?, *Phys. Rev. Lett.* **131**, 240001 (2023).
- [38] J. Provost and G. Vallee, Riemannian structure on manifolds of quantum states, *Commun. Math. Phys.* **76**, 289 (1980).
- [39] Y.-Q. Ma, S. Chen, H. Fan, and W.-M. Liu, Abelian and non-abelian quantum geometric tensor, *Phys. Rev. B* **81**, 245129 (2010).
- [40] M. V. Berry, The quantum phase, five years after, in *Geometric Phases in Physics*, edited by F. Wilczek and E. Shapere (1989) pp. 3–28.
- [41] N. Nagaosa, J. Sinova, S. Onoda, A. H. MacDonald, and N. P. Ong, Anomalous hall effect, *Rev. Mod. Phys.* **82**, 1539 (2010).
- [42] D. Xiao, M.-C. Chang, and Q. Niu, Berry phase effects on electronic properties, *Rev. Mod. Phys.* **82**, 1959 (2010).
- [43] L. Liang, T. I. Vanhala, S. Peotta, T. Siro, A. Harju, and P. Törmä, Band geometry, berry curvature, and superfluid weight, *Phys. Rev. B* **95**, 024515 (2017).
- [44] N. Verma, D. Guerci, and R. Queiroz, Geometric stiffness in interlayer exciton condensates, *Phys. Rev. Lett.* **132**, 236001 (2024).
- [45] X. Hu, T. Hyart, D. I. Pikulin, and E. Rossi, Quantum-metric-enabled exciton condensate in double twisted bilayer graphene, *Phys. Rev. B* **105**, L140506 (2022).
- [46] P. Törmä, L. Liang, and S. Peotta, Quantum metric and effective mass of a two-body bound state in a flat band, *Phys. Rev. B* **98**, 220511 (2018).
- [47] C.-g. Oh, S.-W. Kim, K. W. Kim, B. Monserrat, and J.-W. Rhim, Universal optical conductivity from quantum geometry in quadratic band-touching semimetals, *arXiv preprint arXiv:2503.18372* (2025).
- [48] C.-g. Oh and S.-W. Kim, Color and transparency from quantum geometry, *arXiv preprint arXiv:2507.20904* (2025).
- [49] A. M. Cook, B. M. Fregoso, F. De Juan, S. Coh, and J. E. Moore, Design principles for shift current photovoltaics, *Nat. Commun.* **8**, 14176 (2017).
- [50] F. De Juan, A. G. Grushin, T. Morimoto, and J. E. Moore, Quantized circular photogalvanic effect in Weyl semimetals, *Nat. Commun.* **8**, 15995 (2017).
- [51] P. Bhalla, K. Das, D. Culcer, and A. Agarwal, Resonant second-harmonic generation as a probe of quantum geometry, *Phys. Rev. Lett.* **129**, 227401 (2022).
- [52] B. Ghosh, Y. Onishi, S.-Y. Xu, H. Lin, L. Fu, and A. Bansil, Probing quantum geometry through optical conductivity and magnetic circular dichroism, *Sci. Adv.* **10**, eado1761 (2024).
- [53] M. Ezawa, Analytic approach to quantum metric and optical conductivity in dirac models with parabolic mass in arbitrary dimensions, *Phys. Rev. B* **110**, 195437 (2024).
- [54] J. Ahn, G.-Y. Guo, N. Nagaosa, and A. Vishwanath, Riemannian geometry of resonant optical responses, *Nat. Phys.* **18**, 290 (2022).
- [55] W. Chen, Dielectric and optical markers originating from quantum geometry, *Phys. Rev. B* **111**, 085202 (2025).
- [56] M. Ezawa, Quantum geometry and elliptic optical dichroism in p-wave magnets, *Phys. Rev. B* **112**, 045302 (2025).
- [57] C.-g. Oh, T. Kitamura, A. Daido, J.-W. Rhim, and Y. Yanase, Magnetic phase transitions driven by quantum geometry, *arXiv preprint arXiv:2509.13618* (2025).
- [58] C.-g. Oh, J.-W. Rhim, and B.-J. Yang, Revisiting the magnetic responses of bilayer graphene from the perspective of quantum distance, *Phys. Rev. B* **110**, 155412 (2024).
- [59] T. Kitamura, A. Daido, and Y. Yanase, Spin-triplet superconductivity from quantum-geometry-induced ferromagnetic fluctuation, *Phys. Rev. Lett.* **132**, 036001 (2024).
- [60] J.-W. Rhim, K. Kim, and B.-J. Yang, Quantum distance and anomalous landau levels of flat bands, *Nature* **584**, 59 (2020).
- [61] Y. Hwang, J.-W. Rhim, and B.-J. Yang, Geometric characterization of anomalous landau levels of isolated flat bands, *Nat. Commun.* **12**, 6433 (2021).
- [62] S. Panahiyan, W. Chen, and S. Fritzsche, Fidelity susceptibility near topological phase transitions in quantum walks, *Phys. Rev. B* **102**, 134111 (2020).
- [63] C.-g. Oh, D. Cho, S. Y. Park, and J.-W. Rhim, Bulk-interface correspondence from quantum distance in flat band systems, *Commun. Phys.* **5**, 320 (2022).
- [64] H. Kim, C.-g. Oh, and J.-W. Rhim, General construction scheme for geometrically nontrivial flat band models, *Commun. Phys.* **6**, 305 (2023).
- [65] C.-g. Oh, K. W. Kim, and J.-W. Rhim, Thermoelectric transport driven by the hilbert–schmidt distance, *Adv. Sci.* , 2411313 (2024).
- [66] Y. Xiao and N. Hao, Effects of quantum geometry on the higgs mode in flat-band superconductors, *Phys. Rev. B* **111**, 134502 (2025).
- [67] C.-g. Oh and H. Watanabe, Revisiting electromagnetic response of superconductors in mean-field approximation, *Phys. Rev. Res.* **6**, 013058 (2024).
- [68] K. Katsumi, J. Fiore, M. Udina, R. Romero, D. Barbalas, J. Jesudasan, P. Raychaudhuri, G. Seibold, L. Benfatto, and N. P. Armitage, Revealing Novel Aspects of Light-Matter Coupling by Terahertz Two-Dimensional Coherent Spectroscopy: The Case of the Amplitude Mode in Superconductors, *Phys. Rev. Lett.* **132**, 256903 (2024).
- [69] K. Katsumi, J. Liang, R. Romero, K. Chen, X. Xi, and N. P. Armitage, Amplitude Mode in a Multigap Superconductor MgB_2 Investigated by Terahertz Two-Dimensional Coherent Spectroscopy, *Phys. Rev. Lett.* **135**, 036902 (2025).
- [70] J. Yuan, L. Shi, T. Xu, Y. Wang, Z. Gan, H. Wang, T. Wu, D. Wu, T. Dong, and N. Wang, Selective Excitation of Collective Modes in Multiband Superconductor MgB_2 , *Phys. Rev. Lett.* **135**, 166002 (2025).
- [71] N. Tsuji, Two-dimensional coherent spectroscopy of disordered superconductors in the narrow-band and broad-band limits (2025), *arXiv:2509.03936* [cond-mat.supr-con].

Appendix A: Derivation of the third harmonic generation optical kernel

We start from the Hamiltonian without the electromagnetic field,

$$\mathcal{H} = \mathcal{H}_0 + \mathcal{H}_{\text{int}}, \quad (\text{A1})$$

$$\mathcal{H}_0 = \sum_{\mathbf{k}\sigma\alpha\alpha'} c_{\mathbf{k}\alpha\sigma}^\dagger \mathcal{H}_{\alpha\alpha'}^\sigma(\mathbf{k}) c_{\mathbf{k}\alpha'\sigma}, \quad (\text{A2})$$

$$\mathcal{H}_{\text{int}} = - \sum_{\mathbf{k}\mathbf{k}'\alpha\beta} U_{\alpha\beta} c_{\mathbf{k}\alpha\uparrow}^\dagger c_{-\mathbf{k}\beta\downarrow}^\dagger c_{-\mathbf{k}'\beta\downarrow} c_{\mathbf{k}'\alpha\uparrow}. \quad (\text{A3})$$

We assume the two-body interaction acts only in the Cooper channel between (\mathbf{k}, \uparrow) and $(-\mathbf{k}, \downarrow)$.

Define the finite-temperature partition function

$$\mathcal{Z} = \int \mathcal{D}(c^\dagger, c) e^{-S[c^\dagger, c]}, \quad (\text{A4})$$

$$S[c^\dagger, c] = \int_0^\beta d\tau \left(\sum_{\mathbf{k}\sigma\alpha} c_{\mathbf{k}\alpha\sigma}^\dagger \partial_\tau c_{\mathbf{k}\alpha\sigma} + \mathcal{H} \right). \quad (\text{A5})$$

(For simplicity we set the system volume to unity.)

We decouple \mathcal{H}_{int} by a Hubbard–Stratonovich (HS) transformation in the pairing channel:

$$\begin{aligned} & \exp \left(\sum_{\mathbf{k}\mathbf{k}'\alpha\beta} U_{\alpha\beta} c_{\mathbf{k}\alpha\uparrow}^\dagger c_{-\mathbf{k}\beta\downarrow}^\dagger c_{-\mathbf{k}'\beta\downarrow} c_{\mathbf{k}'\alpha\uparrow} \right) \\ & \rightarrow \int \mathcal{D}(\Delta^*, \Delta) \exp \left(- \sum_{\alpha,\beta} \frac{|\Delta_{\alpha\beta}|^2}{U_{\alpha\beta}} + \sum_{\mathbf{k},\alpha,\beta} (\Delta_{\alpha\beta} c_{\mathbf{k}\alpha\uparrow}^\dagger c_{-\mathbf{k}\beta\downarrow}^\dagger + \text{h.c.}) \right). \end{aligned} \quad (\text{A6})$$

The action becomes

$$\begin{aligned} S[c^\dagger, c, \Delta^*, \Delta] = & \int_0^\beta d\tau \left\{ \sum_{\mathbf{k},\sigma,\alpha,\beta} c_{\alpha\sigma}^\dagger(\mathbf{k}) [(\partial_\tau - \mu)\delta_{\alpha\beta} + \mathcal{H}_{\alpha\beta}^\sigma(\mathbf{k})] c_\beta(\mathbf{k}) \right\} \\ & + \int_0^\beta d\tau \left\{ - \sum_{\mathbf{k},\alpha,\beta} [\Delta_{\alpha\beta} c_{\mathbf{k}\alpha\uparrow}^\dagger c_{-\mathbf{k}\beta\downarrow}^\dagger + \text{h.c.}] + \sum_{\alpha,\beta} \frac{|\Delta_{\alpha\beta}|^2}{U_{\alpha\beta}} \right\}. \end{aligned} \quad (\text{A7})$$

Introduce the vector potential \mathbf{A} by minimal coupling $\mathcal{H}_{\alpha\beta}^\sigma(\mathbf{k}) \rightarrow \mathcal{H}_{\alpha\beta}^\sigma(\mathbf{k} - \mathbf{A})$ (setting $e = c = 1$). Note that for nonlocal electron interactions, the pairing function itself can couple to the gauge field [67]. Assuming a local pairing interaction, only the kinetic term is modified by the vector potential. Then the action with gauge field reads

$$\begin{aligned} S[c^\dagger, c, \Delta^*, \Delta] = & \int_0^\beta d\tau \left\{ \sum_{\mathbf{k},\sigma,\alpha,\beta} c_{\alpha\sigma}^\dagger(\mathbf{k}) [(\partial_\tau - \mu)\delta_{\alpha\beta} + \mathcal{H}_{\alpha\beta}^\sigma(\mathbf{k} - \mathbf{A})] c_\beta(\mathbf{k}) \right\} \\ & + \int_0^\beta d\tau \left\{ - \sum_{\mathbf{k},\alpha,\beta} [\Delta_{\alpha\beta} c_{\mathbf{k}\alpha\uparrow}^\dagger c_{-\mathbf{k}\beta\downarrow}^\dagger + \text{h.c.}] + \sum_{\alpha,\beta} \frac{|\Delta_{\alpha\beta}|^2}{U_{\alpha\beta}} \right\}. \end{aligned} \quad (\text{A8})$$

To analyze the physics in terms of electronic bands, we now perform a change of basis from the orbital basis ($c_{\alpha\sigma}$) to the band basis ($c_{l\sigma}$). Once we use the unitary matrix $u_{l\alpha}^\sigma(\mathbf{k})$ to diagonalize the non-interacting Hamiltonian and find the band dispersions $\epsilon_{l\sigma}(\mathbf{k})$ where l is the band index, we can rewrite the kernel of \mathcal{H}_0 as

$$\mathcal{H}_{\alpha\alpha'}^\sigma(\mathbf{k}) = \sum_l u_{l\alpha}^\sigma(\mathbf{k}) \epsilon_{l\sigma}(\mathbf{k}) u_{l\alpha'}^{\sigma*}(\mathbf{k}). \quad (\text{A9})$$

The transformed fermion operators are $c_{l\sigma\mathbf{A}}(\mathbf{k}) = \sum_\alpha u_{l\alpha}^{\sigma*}(\mathbf{k} - \mathbf{A}) c_{\alpha\sigma}(\mathbf{k})$. Then, the action becomes

$$S[c^\dagger, c, \Delta^*, \Delta] = S_{\text{kin}} + S_{\text{int}}, \quad (\text{A10})$$

where

$$S_{\text{kin}} = \int_0^\beta d\tau \left\{ \sum_{\mathbf{k}, \sigma} \sum_l [\partial_\tau + \epsilon_{l\sigma}(\mathbf{k} - \mathbf{A}) - \mu] c_{l\sigma\mathbf{A}}^\dagger(\mathbf{k}) c_{l\sigma\mathbf{A}}(\mathbf{k}) \right\},$$

$$S_{\text{int}} = \int_0^\beta d\tau \left\{ \sum_{\alpha, \beta} \frac{|\Delta_{\alpha\beta}|^2}{U_{\alpha\beta}} - \sum_{\mathbf{k}, \alpha, \beta, l, l'} \left[\Delta_{\alpha\beta} \left(u_{l\alpha}^*(\mathbf{k} - \mathbf{A}) u_{l'\beta}^\dagger(-\mathbf{k} - \mathbf{A}) \right) c_{l\uparrow\mathbf{A}}^\dagger(\mathbf{k}) c_{l'\downarrow\mathbf{A}}^\dagger(-\mathbf{k}) + h.c. \right] \right\}. \quad (\text{A11})$$

We consider time-reversal symmetry, $u_\alpha^\dagger(-\mathbf{k}) = u_\alpha^*(\mathbf{k})$. Furthermore, we assume that a single band (labeled by index m) near the Fermi level dominates the low-energy physics. We therefore neglect all other bands. For simplicity, we drop the band index m from here on ($c_{m\sigma\mathbf{A}} \rightarrow c_{\sigma\mathbf{A}}, u_{m\alpha} \rightarrow u_\alpha$). We also assume intra-orbital uniform pairing $\Delta_{\alpha\beta} = \Delta \delta_{\alpha\beta}$, which is important to capture quantum-geometric effects on superconductivity [34, 35, 46]. Applying these approximations, the action simplifies to

$$S[c^\dagger, c, \Delta^*, \Delta] = \int_0^\beta d\tau \left\{ N_b \frac{|\Delta|^2}{U} + \sum_{\mathbf{k}, \sigma} [\partial_\tau + \epsilon_\sigma(\mathbf{k} - \mathbf{A}) - \mu] c_{\sigma\mathbf{A}}^\dagger(\mathbf{k}) c_{\sigma\mathbf{A}}(\mathbf{k}) - \sum_{\mathbf{k}} \left[\Delta f(\mathbf{k}, \mathbf{A}) c_{\uparrow\mathbf{A}}^\dagger(\mathbf{k}) c_{\downarrow\mathbf{A}}^\dagger(-\mathbf{k}) + h.c. \right] \right\}, \quad (\text{A12})$$

with

$$f(\mathbf{k}, \mathbf{A}) = \sum_\alpha u_\alpha^*(\mathbf{k} + \mathbf{A}) u_\alpha(\mathbf{k} - \mathbf{A}) = \langle m, \mathbf{k} + \mathbf{A} | m, \mathbf{k} - \mathbf{A} \rangle, \quad (\text{A13})$$

and N_b the number of orbitals. Note that $f(\mathbf{k}, \mathbf{0}) = 1$ and $f^*(\mathbf{k}, \mathbf{A}) = f(\mathbf{k}, -\mathbf{A})$. To second order in \mathbf{A} the overlap is

$$f(\mathbf{k}, \mathbf{A}) = |f(\mathbf{k}, \mathbf{A})| \approx 1 - 2g_{ij}(\mathbf{k}) A_i A_j + \mathcal{O}(A^3), \quad (\text{A14})$$

where $g_{ij}(\mathbf{k})$ is the quantum metric of the Bloch states. Here, we ignore the linear term in A , since it corresponds to the Berry connection. In the presence of both time-reversal and inversion symmetries, the Berry curvature vanishes, allowing for a choice of a real gauge where the Berry connection is locally zero [42]. Even in the presence of global topological obstructions, this linear term possesses odd parity with respect to momentum \mathbf{k} and thus vanishes upon integration over the Brillouin Zone under time-reversal and inversion symmetries. Crucially, this linear term is irrelevant to the third-harmonic generation, which originates from the nonlinear coupling between the Higgs mode and the electromagnetic field ($\sim A^2 \rho$).

Introduce the Nambu spinor $\psi_{\mathbf{k}\mathbf{A}}(\tau) = (c_{\uparrow\mathbf{A}}(\mathbf{k}), c_{\downarrow\mathbf{A}}^\dagger(-\mathbf{k}))^T$. The action becomes

$$S[c^\dagger, c, \Delta^*, \Delta] = \int_0^\beta d\tau \left\{ N_b \frac{|\Delta|^2}{U} + \sum_{\mathbf{k}} \psi_{\mathbf{k}\mathbf{A}}^\dagger(\tau) [-\beta G^{-1}(\mathbf{k}, \tau)] \psi_{\mathbf{k}\mathbf{A}}(\tau) \right\}, \quad (\text{A15})$$

with inverse Nambu propagator

$$G^{-1}(\mathbf{k}, \tau) = \begin{pmatrix} -\partial_\tau - \xi_{\mathbf{k}-\mathbf{A}} & \Delta f(\mathbf{k}, \mathbf{A}) \\ \Delta^* f^*(\mathbf{k}, \mathbf{A}) & -\partial_\tau + \xi_{\mathbf{k}+\mathbf{A}} \end{pmatrix}, \quad \xi_{\mathbf{k}} = \epsilon_{\mathbf{k}} - \mu. \quad (\text{A16})$$

Split the order parameter into its saddle-point and amplitude fluctuation,

$$\Delta(\tau) = \Delta_0 + \rho(\tau),$$

and expand to second order in \mathbf{A} :

$$\xi_{\mathbf{k} \mp \mathbf{A}} = \xi_{\mathbf{k}} + \frac{1}{2} \partial_{ij}^2 \xi_{\mathbf{k}} A_i A_j + \mathcal{O}(A^3). \quad (\text{A17})$$

We assume inversion symmetry $\xi_{\mathbf{k}} = \xi_{-\mathbf{k}}$ so the linear (paramagnetic) term vanishes after \mathbf{k} -integration; only the A^2 diamagnetic term survives in the present context.

Collecting terms, we write

$$S[\rho, c^\dagger, c, A] = \frac{N_b \beta}{U} \Delta_0^2 + \frac{N_b}{U} \int_0^\beta d\tau [\rho(\tau)]^2 + \int_0^\beta d\tau \sum_{\mathbf{k}} \psi_{\mathbf{k}\mathbf{A}}^\dagger(\tau) [-\mathcal{G}^{-1}(\mathbf{k}, \tau)] \psi_{\mathbf{k}\mathbf{A}}(\tau), \quad (\text{A18})$$

with

$$\mathcal{G}^{-1}(\mathbf{k}, \tau) = \mathcal{G}_0^{-1}(\mathbf{k}, \tau) - \Sigma(\mathbf{k}, \tau), \quad (\text{A19})$$

$$\mathcal{G}_0^{-1}(\mathbf{k}, \tau) = -\partial_\tau \tau_0 - \xi_{\mathbf{k}} \tau_3 + \Delta_0 \tau_1, \quad (\text{A20})$$

$$\Sigma(\mathbf{k}, \tau) = \rho(\tau) \tau_1 + \frac{1}{2} \sum_{ij} \partial_{ij}^2 \xi_{\mathbf{k}} A_i(\tau) A_j(\tau) \tau_3 + 2(\Delta_0 + \rho(\tau)) \sum_{ij} g_{ij}(\mathbf{k}) A_i(\tau) A_j(\tau) \tau_1. \quad (\text{A21})$$

Here $\tau_{0,1,2,3}$ are Pauli matrices in Nambu space.

Transform to Matsubara frequency and integrate out fermions using

$$\int D(\psi^\dagger, \psi) e^{-\int \psi^\dagger \mathcal{G}^{-1} \psi} = \det(\beta \mathcal{G}^{-1}) = \exp(\text{Tr} \ln[\beta \mathcal{G}^{-1}]). \quad (\text{A22})$$

Expanding the fermion determinant to quartic order in fields (i.e. up to $O(A^4)$ and quadratic in ρ), using $\ln[\beta \mathcal{G}^{-1}] = \ln[\beta \mathcal{G}_0] + \sum_{n=1}^{\infty} \frac{(-1)^{2n-1}}{n} (\mathcal{G}_0 \Sigma)^{2n}$, and collecting terms relevant for third-harmonic generation, one obtains

$$\begin{aligned} S^{(2)}[\rho, A] = & \frac{\beta}{2} \sum_{i\omega_n} \rho^*(i\omega_n) [\mathcal{G}_H^0]^{-1}(i\omega_n) \rho(i\omega_n) \\ & - \frac{\beta}{2} \sum_{i\omega_m} [\rho^*(i\omega_m) b(i\omega_m) + b^*(i\omega_m) \rho(i\omega_m)] \\ & + \frac{\beta}{2} \sum_{\mathbf{k}, i\omega_m} \frac{1}{4} \partial_{ij}^2 \xi_{\mathbf{k}} \partial_{kl}^2 \xi_{\mathbf{k}} \chi_{33}(\mathbf{k}, i\omega_m) A_{ij}^2(-i\omega_m) A_{kl}^2(i\omega_m) \\ & + \frac{\beta}{2} \sum_{\mathbf{k}, i\omega_m} 2 \Delta_0 \partial_{ij}^2 \xi_{\mathbf{k}} g_{kl}(\mathbf{k}) \chi_{13}(\mathbf{k}, -i\omega_m) A_{ij}^2(-i\omega_m) A_{kl}^2(i\omega_m) \\ & + \frac{\beta}{2} \sum_{\mathbf{k}, i\omega_m} 4 \Delta_0^2 g_{ij}(\mathbf{k}) g_{kl}(\mathbf{k}) \chi_{11}(\mathbf{k}, i\omega_m) A_{ij}^2(-i\omega_m) A_{kl}^2(i\omega_m), \end{aligned} \quad (\text{A23})$$

where $\chi_{\alpha\beta}(\mathbf{k}, i\omega_m) = \frac{1}{\beta} \sum_{i\omega_n} \text{Tr}[\mathcal{G}_0(\mathbf{k}, i\omega_n) \tau_\alpha \mathcal{G}_0(\mathbf{k}, i\omega_n + i\omega_m) \tau_\beta]$. The Higgs inverse propagator and source are

$$[\mathcal{G}_H^0(i\omega_n)]^{-1} = \frac{2}{U} + \sum_{\mathbf{k}} \chi_{11}(\mathbf{k}, i\omega_n), \quad (\text{A24})$$

$$\begin{aligned} b(i\omega_m) = & \frac{1}{2} \sum_{\mathbf{k}} \sum_{ij} \partial_{ij}^2 \xi_{\mathbf{k}} \chi_{13}(\mathbf{k}, i\omega_m) A_{ij}^2(i\omega_m) \\ & + 2 \sum_{\mathbf{k}} \sum_{ij} \Delta_0 g_{ij}(\mathbf{k}) \chi_{11}(\mathbf{k}, i\omega_m) A_{ij}^2(i\omega_m). \end{aligned} \quad (\text{A25})$$

In the above, $A_{ij}^2(i\omega)$ denotes the Fourier transform of $A_i(\tau) A_j(\tau)$:

$$A_{ij}^2(i\omega) \equiv \frac{1}{\beta} \int_0^\beta d\tau e^{i\omega\tau} A_i(\tau) A_j(\tau), \quad (\text{A26})$$

which is not equal to $A_i(i\omega) A_j(i\omega)$ in general.

Integrating out the Higgs field ρ by completing the square yields

$$\int D[\rho] \exp\left(\frac{1}{2} \rho^\dagger \mathcal{G}_H^{-1} \rho + \frac{1}{2} \rho^\dagger b + \frac{1}{2} b^\dagger \rho\right) = \mathcal{N} \det(\mathcal{G}_H) \exp\left(\frac{1}{2} b^\dagger \mathcal{G}_H b\right). \quad (\text{A27})$$

After analytic continuation $i\omega \rightarrow \omega + i0^+$ and rearranging, the effective electromagnetic action can be written as

$$S[A] = \sum_{ijkl} \int d\omega A_{ij}^2(-\omega) K_{ijkl}(\omega) A_{kl}^2(\omega), \quad (\text{A28})$$

with the optical kernel decomposed as

$$K_{ijkl}(\omega) = K_{ijkl}^{\text{qp}}(\omega) + K_{ijkl}^{\text{Higgs}}(\omega). \quad (\text{A29})$$

The quasiparticle contribution is

$$K_{ijkl}^{\text{qp}}(\omega) = \sum_{\mathbf{k}} \left[\frac{1}{4} \partial_{ij}^2 \xi_{\mathbf{k}} \partial_{kl}^2 \xi_{\mathbf{k}} \chi_{33}(\mathbf{k}, \omega) + 2 \Delta_0 \partial_{ij}^2 \xi_{\mathbf{k}} g_{kl}(\mathbf{k}) \chi_{13}(\mathbf{k}, \omega) + 4 \Delta_0^2 g_{ij}(\mathbf{k}) g_{kl}(\mathbf{k}) \chi_{11}(\mathbf{k}, \omega) \right], \quad (\text{A30})$$

and the Higgs-mediated contribution is

$$K_{ijkl}^{\text{Higgs}}(\omega) = - \left[\frac{1}{2} \sum_{\mathbf{k}} \partial_{ij}^2 \xi_{\mathbf{k}} \chi_{13}(\mathbf{k}, \omega) + 2 \Delta_0 \sum_{\mathbf{k}} g_{ij}(\mathbf{k}) \chi_{11}(\mathbf{k}, \omega) \right] \times \mathcal{G}_H^0(\omega) \left[\frac{1}{2} \sum_{\mathbf{k}'} \partial_{kl}^2 \xi_{\mathbf{k}'} \chi_{13}(\mathbf{k}', \omega) + 2 \Delta_0 \sum_{\mathbf{k}'} g_{kl}(\mathbf{k}') \chi_{11}(\mathbf{k}', \omega) \right]. \quad (\text{A31})$$

At zero temperature one obtains closed forms for the bubbles (retarded continuation). For example,

$$\chi_{11}(\mathbf{k}, \omega) = - \frac{4\xi_{\mathbf{k}}^2}{E_{\mathbf{k}}(4E_{\mathbf{k}}^2 - \omega^2)}, \quad (\text{A32})$$

$$\chi_{13}(\mathbf{k}, \omega) = - \frac{4\xi_{\mathbf{k}}\Delta_0}{E_{\mathbf{k}}(4E_{\mathbf{k}}^2 - \omega^2)}, \quad (\text{A33})$$

$$\chi_{33}(\mathbf{k}, \omega) = - \frac{4\Delta_0^2}{E_{\mathbf{k}}(4E_{\mathbf{k}}^2 - \omega^2)}, \quad (\text{A34})$$

with $E_{\mathbf{k}} = \sqrt{\xi_{\mathbf{k}}^2 + \Delta_0^2}$. These forms follow from evaluating the Matsubara sums and performing analytic continuation; they satisfy $\chi_{11} + \chi_{33} = -4/(4E^2 - \omega^2)$ and χ_{13} is the mixed numerator $\propto \xi\Delta$.

The Higgs propagator reads

$$\mathcal{G}_H^0(\omega) = \left[2\rho_0 \arcsin\left(\frac{\omega}{2\Delta_0}\right) \right]^{-1} \left[\left(\frac{2\Delta_0}{\omega}\right)^2 - 1 \right]^{-1/2}, \quad (\text{A35})$$

where ρ_0 denotes the density-of-states factor entering the amplitude fluctuation kernel.

The electromagnetic current is obtained by functional differentiation

$$j_m(t) = - \frac{\delta S}{\delta A_m(t)}.$$

Working in the frequency domain and using the quartic effective action $S[A]$ above, for a monochromatic drive

$$A_i(t) = a_i e^{-i\Omega t} + a_i^* e^{i\Omega t},$$

the 3Ω component of the current is

$$\begin{aligned} j_m(3\Omega) &= -4 \sum_{jkl} K_{mjkl}(2\Omega) a_j a_k a_l \\ &= -4 \sum_{jkl} [K_{mjkl}^{\text{qp}}(2\Omega) + K_{mjkl}^{\text{Higgs}}(2\Omega)] a_j a_k a_l. \end{aligned} \quad (\text{A36})$$

Appendix B: Derivation of the Higgs correlation Length

To derive the correlation length, we start from the action with a static, spatially varying order parameter $\Delta(q)$ and no external field ($\mathbf{A} = 0$). The Hamiltonian is given by

$$\mathcal{H} = \mathcal{H}_0 + \mathcal{H}_{\text{int}}, \quad (\text{B1})$$

$$\mathcal{H}_0 = \sum_{\mathbf{k}\sigma\alpha\alpha'} c_{\mathbf{k}\alpha\sigma}^\dagger \mathcal{H}_{\alpha\alpha'}^\sigma(\mathbf{k}) c_{\mathbf{k}\alpha'\sigma}, \quad (\text{B2})$$

$$\mathcal{H}_{\text{int}} = - \sum_{\mathbf{k}\mathbf{k}'\alpha\beta} U_{\alpha\beta} c_{\mathbf{k}+\mathbf{q}\alpha\uparrow}^\dagger c_{-\mathbf{k}\beta\downarrow}^\dagger c_{-\mathbf{k}'\beta\downarrow} c_{\mathbf{k}'+\mathbf{q}\alpha\uparrow}. \quad (\text{B3})$$

The partition function \mathcal{Z} and the action are written as

$$\mathcal{Z} = \int \mathcal{D}(c^\dagger, c) e^{-S[c^\dagger, c]}, \quad S[c^\dagger, c] = \int_0^\beta d\tau \left(\sum_{\mathbf{k}\sigma\alpha} c_{\mathbf{k}\alpha\sigma}^\dagger \partial_\tau c_{\mathbf{k}\alpha\sigma} + \mathcal{H} \right). \quad (\text{B4})$$

We decouple the interaction term using a Hubbard-Stratonovich transformation in the pairing channel:

$$\begin{aligned} & \exp \left(\sum_{\mathbf{k}\mathbf{k}'\alpha\beta} U_{\alpha\beta} c_{\mathbf{k}+\mathbf{q}\alpha\uparrow}^\dagger c_{-\mathbf{k}\beta\downarrow}^\dagger c_{-\mathbf{k}'\beta\downarrow} c_{\mathbf{k}'+\mathbf{q}\alpha\uparrow} \right) \\ & \rightarrow \int \mathcal{D}(\Delta^*, \Delta) \exp \left(- \sum_{\alpha,\beta,\mathbf{q}} \frac{|\Delta_{\alpha\beta}(\mathbf{q})|^2}{U_{\alpha\beta}} + \sum_{\mathbf{k},\mathbf{q},\alpha,\beta} (\Delta_{\alpha\beta}(\mathbf{q}) c_{\mathbf{k}+\mathbf{q}\alpha\uparrow}^\dagger c_{-\mathbf{k}\beta\downarrow}^\dagger + h.c.) \right). \end{aligned} \quad (\text{B5})$$

Then the action becomes

$$\begin{aligned} S[c^\dagger, c, \Delta^*, \Delta] = & \int_0^\beta d\tau \left\{ \sum_{\mathbf{k},\sigma,\alpha,\beta} c_{\mathbf{k}\alpha\sigma}^\dagger [(\partial_\tau - \mu)\delta_{\alpha\beta} + \mathcal{H}_{\alpha\beta}^\sigma] c_{\mathbf{k}\beta}(\mathbf{k}) \right\} \\ & + \int_0^\beta d\tau \left\{ - \sum_{\mathbf{k},\mathbf{q},\alpha,\beta} [\Delta_{\alpha\beta}(\mathbf{q}) c_{\mathbf{k}+\mathbf{q}\alpha\uparrow}^\dagger c_{-\mathbf{k}\beta\downarrow}^\dagger + h.c.] + \sum_{\mathbf{q},\alpha,\beta} \frac{|\Delta_{\alpha\beta}(\mathbf{q})|^2}{U_{\alpha\beta}} \right\} \end{aligned} \quad (\text{B6})$$

To analyze the physics in terms of electronic bands, we now perform a change of basis from the orbital basis ($c_{\alpha\sigma}$) to the band basis ($c_{l\sigma}$). We then make key approximations: (i) we project the theory onto a single dominant band (labeled m , which we drop hereafter) near the Fermi level, (ii) we assume a uniform, intra-orbital pairing form, $\Delta_{\alpha\beta}(q) = \Delta(q)\delta_{\alpha\beta}$, and (iii) time-reversal symmetry. Applying these approximations, the action simplifies.

$$\begin{aligned} S[c^\dagger, c, \Delta^*, \Delta] = & \beta N_b \sum_{\mathbf{q}} \frac{|\Delta(\mathbf{q})|^2}{U} + \beta \sum_{\mathbf{k},\sigma} [-i\omega_n + \epsilon_\sigma(\mathbf{k}) - \mu] c_\sigma^\dagger(\mathbf{k}) c_\sigma(\mathbf{k}) \\ & - \beta \sum_{\mathbf{k},\mathbf{q}} \left[\Delta(\mathbf{q}) f(\mathbf{k}, \mathbf{q}) c_\uparrow^\dagger(\mathbf{k}) c_\downarrow^\dagger(-\mathbf{k} + \mathbf{q}) + h.c. \right], \end{aligned} \quad (\text{B7})$$

where $f(\mathbf{k}, \mathbf{q}) = \sum_\alpha u_\alpha^*(\mathbf{k}) u_\alpha(\mathbf{k} - \mathbf{q}) = \langle m, \mathbf{k} | m, \mathbf{k} - \mathbf{q} \rangle$, which satisfies $f(\mathbf{k}, \mathbf{0}) = 1$, $f(\mathbf{k}, \mathbf{q}) \approx 1 - g_{ij}(\mathbf{k}) q_i q_j / 2 + O(q^4)$, and N_b is the number of orbitals.

By introducing the Nambu spinor $\psi(k) = (c_\uparrow(k) \ c_\downarrow^\dagger(-k))^T$, the action can be written in a BdG form as

$$S[c^\dagger, c, \Delta^*, \Delta] = \beta N_b \sum_{\mathbf{q}} \frac{|\Delta(\mathbf{q})|^2}{U} + \sum_{\mathbf{k},\mathbf{q}} \psi^\dagger(\mathbf{k}) [-\beta \mathcal{G}^{-1}(\mathbf{k}, \mathbf{k} - \mathbf{q})] \psi(\mathbf{k} - \mathbf{q}). \quad (\text{B8})$$

The inverse Nambu propagator \mathcal{G}^{-1} is identified as

$$\mathcal{G}^{-1}(\mathbf{k}, \mathbf{k} - \mathbf{q}) = \begin{pmatrix} (i\omega_n - \xi_{\mathbf{k}})\delta_{q,0} & \Delta(\mathbf{q})f(\mathbf{k}, \mathbf{q}) \\ \Delta^*(-\mathbf{q})f^*(\mathbf{k} - \mathbf{q}, -\mathbf{q}) & (i\omega_n + \xi_{\mathbf{k}})\delta_{q,0} \end{pmatrix} \quad (\text{B9})$$

where $\xi_{\mathbf{k}} = \epsilon_{\mathbf{k}} - \mu$.

We expand the order parameter field around the mean-field saddle point as

$$\Delta(q) = \Delta_0 \delta_{q,0} + \rho(q) + i\Delta_0 \theta(q), \quad (\text{B10})$$

where ρ is the amplitude fluctuation and θ the phase fluctuation.

Then the propagator in Eq. (B9) becomes $\mathcal{G}^{-1} = \mathcal{G}_0^{-1} + \Sigma$, where

$$\mathcal{G}_0^{-1}(k) = \begin{pmatrix} i\omega_n - \xi_{\mathbf{k}} & \Delta_0 \\ \Delta_0 & i\omega_n + \xi_{\mathbf{k}} \end{pmatrix}, \quad (\text{B11})$$

$$\Sigma(k, q) = A(q) f(\mathbf{k}, \mathbf{q}) \tau_+ + A^*(-q) f^*(\mathbf{k} - \mathbf{q}, -\mathbf{q}) \tau_-, \quad (\text{B12})$$

where $\tau_{\pm} = (\tau_1 \pm i\tau_2)/2$ and $A(q) = \rho(q) + i\Delta_0 \theta(q)$. Note that $\theta(q) = \theta^*(-q)$, $\rho(q) = \rho^*(-q)$, since $\theta(x)$ and $\rho(x)$ are both real fields, and $f(\mathbf{k} - \mathbf{q}, -\mathbf{q}) = f(\mathbf{k}, \mathbf{q}) = 1 - g_{ij}(\mathbf{k}) q_i q_j / 2$ up to second order in \mathbf{q} .

Integrating out the fermionic fields, we write down the effective theory for the order parameters as

$$S_{\text{eff}}[\Delta^*, \Delta] = \beta N_b \sum_q \frac{|\Delta(q)|^2}{U} + \beta \sum_{\mathbf{k}} \xi_{\mathbf{k}} - \text{Tr} \ln[\beta \mathcal{G}^{-1}] \quad (\text{B13})$$

Since $\ln[\beta \mathcal{G}^{-1}] = \ln[\beta \mathcal{G}_0] + \sum_{n=1}^{\infty} \frac{(-1)^{2n-1}}{n} (\mathcal{G}_0 \Sigma)^{2n}$, the action of the order quadratic ρ , i.e., $O(\rho^2)$, can be written as

$$S^{(2)} = \beta N_b \sum_q \frac{|\Delta(q)|^2}{U} + \frac{1}{2} \text{Tr}[\mathcal{G}_0 \Sigma \mathcal{G}_0 \Sigma]. \quad (\text{B14})$$

We consider static $q_0 = 0$. Furthermore, for simplicity, we introduce the dimensionless Higgs field $h(q) \equiv \rho(q)/\Delta_0$. A straightforward calculation leads to

$$S^{(2)} = \sum_{\mathbf{q}} \begin{pmatrix} h(-\mathbf{q}) & \theta(-\mathbf{q}) \end{pmatrix} \Gamma(\mathbf{q}) \begin{pmatrix} h(\mathbf{q}) \\ \theta(\mathbf{q}) \end{pmatrix}, \quad (\text{B15})$$

where

$$\Gamma(\mathbf{q}) \simeq \begin{pmatrix} r_{\rho} + A_{ij} q_i q_j & 0 \\ 0 & r_{\theta} + B_{ij} q_i q_j \end{pmatrix} + O(q^4), \quad (\text{B16})$$

with

$$r_{\rho} = \frac{N_b \Delta_0^2}{U} - \frac{\Delta_0^2}{2} \sum_{\mathbf{k}} \frac{\xi_{\mathbf{k}}^2}{E_{\mathbf{k}}^3} = \frac{\Delta_0^4}{2} \sum_{\mathbf{k}} \frac{1}{E_{\mathbf{k}}^3}, \quad (\text{B17})$$

$$r_{\theta} = \frac{N_b \Delta_0^2}{U} - \frac{\Delta_0^2}{2} \sum_{\mathbf{k}} \frac{1}{E_{\mathbf{k}}} = 0, \quad (\text{B18})$$

$$A_{ij} = \sum_{\mathbf{k}} \left[v_i(\mathbf{k}) v_j(\mathbf{k}) \frac{\Delta_0^2}{8E_{\mathbf{k}}^7} (-\Delta_0^4 + 8\Delta_0^2 \xi_{\mathbf{k}}^2 - \xi_{\mathbf{k}}^4) + \xi_{ij}(\mathbf{k}) \frac{\xi_{\mathbf{k}} \Delta_0^2}{8E_{\mathbf{k}}^5} (-2\Delta_0^2 + \xi_{\mathbf{k}}^2) + g_{ij}(\mathbf{k}) \frac{\Delta_0^2}{2} \frac{\xi_{\mathbf{k}}^2}{E_{\mathbf{k}}^3} \right], \quad (\text{B19})$$

$$B_{ij} = \sum_{\mathbf{k}} \left[v_i(\mathbf{k}) v_j(\mathbf{k}) \frac{\Delta_0^2}{8E_{\mathbf{k}}^5} (2\Delta_0^2 - \xi_{\mathbf{k}}^2) + \xi_{ij}(\mathbf{k}) \frac{\xi_{\mathbf{k}} \Delta_0^2}{8E_{\mathbf{k}}^3} + g_{ij}(\mathbf{k}) \frac{\Delta_0^2}{2} \frac{1}{E_{\mathbf{k}}} \right], \quad (\text{B20})$$

where $v_i(\mathbf{k}) = \partial_i \xi_{\mathbf{k}}$ and $\xi_{ij}(\mathbf{k}) = \partial_i \partial_j \xi_{\mathbf{k}}$. For these calculations, we use

$$T_{11} \equiv \text{Tr}[\mathcal{G}_0(k+q)\tau_1\mathcal{G}_0(k)\tau_1] = \frac{2(\Delta_0^2 - \omega^2 - \xi_k\xi_{k+q})}{(\omega^2 + E_{k+q}^2)(\omega^2 + E_k^2)}, \quad (\text{B21})$$

$$T_{22} \equiv \text{Tr}[\mathcal{G}_0(k+q)\tau_2\mathcal{G}_0(k)\tau_2] = \frac{2(-\Delta_0^2 - \omega^2 - \xi_k\xi_{k+q})}{(\omega^2 + E_{k+q}^2)(\omega^2 + E_k^2)}, \quad (\text{B22})$$

$$T_{12} \equiv \text{Tr}[\mathcal{G}_0(k+q)\tau_1\mathcal{G}_0(k)\tau_2] = \frac{2\omega(\xi_{k+q} - \xi_k)}{(\omega^2 + E_{k+q}^2)(\omega^2 + E_k^2)}, \quad (\text{B23})$$

$$\frac{1}{\beta} \sum_{i\omega_n} \frac{1}{\omega_n^2 + E^2} = \frac{1}{2E}, \quad \frac{1}{\beta} \sum_{i\omega_n} \frac{1}{(\omega_n^2 + E^2)(\omega_n^2 + E'^2)} = \frac{1}{2EE'(E + E')}, \quad (\text{B24})$$

$$\Pi_{11}(k, k+q) \equiv \frac{1}{\beta} \sum_{i\omega_n} T_{11} = \frac{\Delta_0^2 - E_k E_{k+q} - \xi_k \xi_{k+q}}{E_k E_{k+q} (E_k + E_{k+q})}, \quad (\text{B25})$$

$$\Pi_{22}(k, k+q) \equiv \frac{1}{\beta} \sum_{i\omega_n} T_{22} = \frac{-\Delta_0^2 - E_k E_{k+q} - \xi_k \xi_{k+q}}{E_k E_{k+q} (E_k + E_{k+q})}. \quad (\text{B26})$$

Thus, the correlation length is

$$\langle h(\mathbf{q})h(-\mathbf{q}) \rangle \propto \frac{1}{r_\rho + A_{ij}q_i q_j}, \quad (\text{B27})$$

$$\xi_{H,ij}^2 = \frac{A_{ij}}{r_\rho} = \xi_{\text{band},ij}^2 + \xi_{\text{geom},ij}^2, \quad (\text{B28})$$

$$\xi_{\text{band},ij}^2 = \frac{1}{r_\rho} \sum_{\mathbf{k}} \left[v_i(\mathbf{k})v_j(\mathbf{k}) \frac{\Delta_0^2}{8E_{\mathbf{k}}^7} (-\Delta_0^4 + 8\Delta_0^2 \xi_{\mathbf{k}}^2 - \xi_{\mathbf{k}}^4) + \xi_{ij}(\mathbf{k}) \frac{\xi_{\mathbf{k}} \Delta_0^2}{8E_{\mathbf{k}}^5} (-2\Delta_0^2 + \xi_{\mathbf{k}}^2) \right], \quad (\text{B29})$$

$$\xi_{\text{geom},ij}^2 = \frac{1}{r_\rho} \sum_{\mathbf{k}} g_{ij}(\mathbf{k}) \frac{\Delta_0^2}{2} \frac{\xi_{\mathbf{k}}^2}{E_{\mathbf{k}}^3} \quad (\text{B30})$$

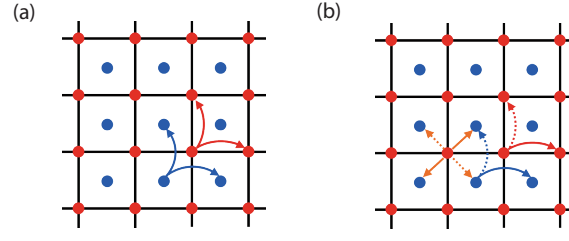


FIG. 3. Real-space lattice models for (a) $d_{\max} = 0$ and (b) $d_{\max} = 1$.

Appendix C: Quadratic Band Touching Model

The non-interacting Hamiltonian for the tunable quadratic band touching model used in the main text is given by

$$\mathcal{H}^\dagger(\mathbf{k}) = \mathcal{H}^{\downarrow*}(-\mathbf{k}) = h_0(\mathbf{k})\tau_0 + \mathbf{h}(\mathbf{k}) \cdot \boldsymbol{\tau}, \quad (\text{C1})$$

where the components are defined as:

$$\begin{aligned} h_0(\mathbf{k}) &= -2(t - t_b) - (t_b + t)(\cos k_x + \cos k_y), \\ h_x(\mathbf{k}) &= 4d_{\max}(t - t_b)\sin(k_x/2)\sin(k_y/2), \\ h_y(\mathbf{k}) &= -2d_{\max}\sqrt{1 - d_{\max}^2}(t - t_b)(\cos k_y - 1), \\ h_z(\mathbf{k}) &= (t - t_b)[2(1 - d_{\max}^2) - \cos k_x + (2d_{\max}^2 - 1)\cos k_y]. \end{aligned}$$

This specific construction ensures time-reversal symmetry and that the band dispersions, $E_{\pm}(\mathbf{k})$, are independent of the parameter d_{\max} , which solely controls the quantum geometry of the Bloch states. The quantum metric for the upper band is given by $g_{xx}(\mathbf{k}) = d_{\max}^2 \cos^2(k_x/2) \sin^2(k_y/2) / \mathcal{D}(\mathbf{k})^2$, $g_{xy}(\mathbf{k}) = -d_{\max}^2 \sin k_x \sin k_y / (4\mathcal{D}(\mathbf{k})^2)$, $g_{yy}(\mathbf{k}) = d_{\max}^2 \cos^2(k_y/2) \sin^2(k_x/2) / \mathcal{D}(\mathbf{k})^2$, where $\mathcal{D}(\mathbf{k}) = -2 + \cos k_x + \cos k_y$. Note that these expressions defined for $\mathbf{k} \neq \mathbf{0}$.

Real-Space Lattice Representations

While the k -space Hamiltonian is well-defined for any d_{\max} , it is instructive to examine the real-space tight-binding models that correspond to the two limiting cases.

Geometrically trivial limit ($d_{\max} = 0$)

In this case, the model describes two uncoupled orbitals (A and B) on a square lattice, each with simple nearest-neighbor hopping. The real-space Hamiltonian is:

$$H = \sum_{\mathbf{R}} [\epsilon_A a_{\mathbf{R}}^\dagger a_{\mathbf{R}} + \epsilon_B b_{\mathbf{R}}^\dagger b_{\mathbf{R}}] + \sum_{\mathbf{R}, \nu=x,y} [-t a_{\mathbf{R}}^\dagger a_{\mathbf{R}+\hat{\nu}} - t_b b_{\mathbf{R}}^\dagger b_{\mathbf{R}+\hat{\nu}} + \text{h.c.}], \quad (\text{C2})$$

where $\epsilon_A = 0$ and $\epsilon_B = 4(t_b - t)$ are the on-site energies. This lattice is depicted in Fig. 3(a).

Maximally nontrivial limit ($d_{\max} = 1$)

This limit maps onto a more complex tight-binding model with anisotropic hopping and intricate, spatially dependent inter-orbital couplings. The Hamiltonian is:

$$\begin{aligned} \mathcal{H} &= \sum_{\mathbf{R}} [\epsilon_A a_{\mathbf{R}}^\dagger a_{\mathbf{R}} + \epsilon_B b_{\mathbf{R}}^\dagger b_{\mathbf{R}}] + \sum_{\mathbf{R}, \nu=x,y} [t_{A,\nu} a_{\mathbf{R}}^\dagger a_{\mathbf{R}+\hat{\nu}} + t_{B,\nu} b_{\mathbf{R}}^\dagger b_{\mathbf{R}+\hat{\nu}} + \text{h.c.}] \\ &\quad + \sum_{\mathbf{R}} [A(a_{\mathbf{R}}^\dagger b_{\mathbf{R}} - a_{\mathbf{R}}^\dagger b_{\mathbf{R}-\hat{x}} - a_{\mathbf{R}}^\dagger b_{\mathbf{R}-\hat{y}} + a_{\mathbf{R}}^\dagger b_{\mathbf{R}-\hat{x}-\hat{y}}) + \text{h.c.}], \end{aligned} \quad (\text{C3})$$

where the parameters are $\epsilon_A = \epsilon_B = 2(t_b - t)$, $t_{A,x} = t_{B,y} = -t$, $t_{A,y} = t_{B,x} = -t_b$, and $A = t_b - t$. This structure is shown in Fig. 3(b).

Intermediate regime ($0 < d_{\max} < 1$)

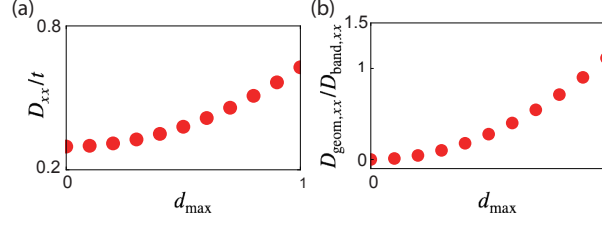


FIG. 4. Quantum geometric enhancement of the superfluid stiffness. (a) Superfluid weight D_{xx} within the quadratic band touching model. (b) The ratio of the geometric to the band contribution to D_{xx} . The parameters $\mu, \Delta_0/W$ are the same as in Fig. 1(b,c) of the main text.

For intermediate values of d_{\max} , constructing a corresponding local tight-binding model on a simple square lattice is challenging. However, the k -space model, which is mathematically well-defined across the entire range of d_{\max} , provides the essential theoretical framework for demonstrating how the system's properties are smoothly governed by the underlying quantum geometry.

Appendix D: Superfluid stiffness

We calculate the superfluid stiffness from the effective action in Eq. (A18). To obtain the superfluid stiffness, we expand the action to $O(A^2)$. Taking $\rho = 0$ for the static stiffness, the A^2 self-energy becomes

$$\Sigma_{A^2}(\mathbf{k}) = \frac{1}{2} \sum_{ij} \partial_{ij}^2 \xi_{\mathbf{k}} A_i A_j \tau_3 + 2\Delta_0 \sum_{ij} g_{ij}(\mathbf{k}) A_i A_j \tau_1. \quad (\text{D1})$$

Since Σ_{A^2} is already $O(A^2)$, the quadratic electromagnetic action is

$$S_{\text{eff}}^{(A^2)} = \text{Tr}[\mathcal{G}_0 \Sigma_{A^2}] + O(A^4). \quad (\text{D2})$$

The required Nambu traces are

$$\text{Tr}[\mathcal{G}_0 \tau_3] = \frac{2\xi_{\mathbf{k}}}{(i\omega_n)^2 - E_{\mathbf{k}}^2}, \quad \text{Tr}[\mathcal{G}_0 \tau_1] = -\frac{2\Delta_0}{(i\omega_n)^2 - E_{\mathbf{k}}^2}. \quad (\text{D3})$$

Using the Matsubara identity

$$\frac{1}{\beta} \sum_{i\omega_n} \frac{1}{(i\omega_n)^2 - E^2} = -\frac{1}{2E} \tanh\left(\frac{\beta E}{2}\right), \quad (\text{D4})$$

so that at $T = 0$,

$$S_{\text{eff}}^{(A^2)} = \frac{\beta}{2} \sum_{ij} A_i \left(\sum_{\mathbf{k}} -\frac{\xi_{\mathbf{k}} \partial_{ij}^2 \xi_{\mathbf{k}}}{E_{\mathbf{k}}} + \frac{4\Delta_0^2 g_{ij}(\mathbf{k})}{E_{\mathbf{k}}} \right) A_j. \quad (\text{D5})$$

Thus, the superfluid stiffness D_{ij} reads

$$D_{ij} = \sum_{\mathbf{k}} \left[-\frac{\xi_{\mathbf{k}} \partial_{ij}^2 \xi_{\mathbf{k}}}{E_{\mathbf{k}}} + \frac{4\Delta_0^2 g_{ij}(\mathbf{k})}{E_{\mathbf{k}}} \right]. \quad (\text{D6})$$

The first and second terms corresponds to D_{ij}^{band} and D_{ij}^{geom} , respectively. This result is identical to that found in [34, 43].

Figure 4 shows the d_{\max} -dependence of the superfluid stiffness for the same parameters as in Fig. 1(b,c) of the main text. As d_{\max} increases, the superfluid stiffness is enhanced.